

Article

# Combining Airborne and Terrestrial Laser Scanning Technologies to Measure Forest Understorey Volume

Luxia Liu <sup>1</sup>, Yong Pang <sup>1,\*</sup>, Zengyuan Li <sup>1</sup>, Lin Si <sup>1</sup> and Shengxi Liao <sup>2</sup>

<sup>1</sup> Institute of Forest Resource Information Techniques, Chinese Academy of Forestry, Beijing 100091, China; lucia.liu.caf@gmail.com (L.L.); lizengyuan@ifrit.ac.cn (Z.L.); silin@ifrit.ac.cn (L.S.)

<sup>2</sup> The Research Institute of Resources Insects, Chinese Academy of Forestry, Kunming 650224, China; cafliao@163.com

\* Correspondence: pangy@ifrit.ac.cn

Academic Editors: Juha Hyppä and Timothy A. Martin

Received: 17 January 2017; Accepted: 1 April 2017; Published: 6 April 2017

**Abstract:** A critical component of the forest ecosystem, the understorey supports the vast majority of wildlife habitat and total ecosystem floristic diversity. Remote sensing data have been developed to provide information at different scales for surveys of forest ecosystems, but obtaining information about the understorey remains a challenge. As rapid and efficient tools for forest structure attribute estimation, Airborne Laser Scanning (ALS) and Terrestrial Laser Scanning (TLS) have attracted much attention. We examine the relationship between ALS and TLS data and detect changes in the forest understorey caused by forest-tending events in the study area. We conducted trials in five plots within a young Khasi pine (*Pinus kesiya* Royle ex Gord.) plantation in Yunnan province, China, before and after forest tending. We collected bi-temporal ALS data in this area and TLS data from 10 scanning stations. Canopy height profiles were retrieved from ALS and TLS data, and understorey material volume retrieved from filled TLS voxels volume agreed well with the understorey point clouds percentile distribution (PD) obtained from ALS data. The PD value for the understorey from ALS multiplied by the percentage of ALS return points in the overstorey had a stronger correlation ( $R^2 = 0.90$ ) with the TLS-derived understorey material volume than did the ALS PD value for the understorey only ( $R^2 = 0.71$ ). Taking the effect of the overstorey into consideration will improve evaluations of forest understorey parameters from ALS data. This study confirmed the potential of TLS as a validation tool to assess the accuracy of forest understorey material volume estimation at large scales using ALS data.

**Keywords:** ALS; canopy height profile; change detection; forest tending; forest understorey monitoring; TLS

## 1. Introduction

Although understorey species contain less than 1% of the aboveground biomass of tropical forests in the Northern Hemisphere, they play a critical role in supporting global ecosystem services [1]. The vast majority of plant species in north-temperate forests and plantations are not overstorey tree canopy but rather understorey herbs, shrubs, and subshrubs [2]. As a critical component of the forest ecosystem, the understorey layer supports ecosystem floristic diversity, wildlife species, and ecosystem services such as carbon sequestration [3]. The dynamics of the understorey layer are closely associated with long-term forest successional patterns [4]. Earlier studies have suggested that forest understorey layers can interact with the overstorey canopy, affect species regeneration [5,6], contribute to forest biodiversity, and influence energy fluxes and nutrient cycles [7].

Within forest stands, differences in vegetation composition, structure, and foliage distribution create spatial variation in light transmittance to the understorey, affecting the growth and mortality

of tree seedlings and saplings [8]. Because canopy structure remains poorly defined at the stand scale, there is a need for ecologists to understand how tree crowns occupy the three-dimensional (3D) space of the canopy layer and how the understorey environment is influenced by canopy structure [9]. Therefore, the estimation of the composition, structure, and foliage distribution of understorey vegetation is especially important for research on forest ecosystem function and services. Conventionally, information on the forest understorey is obtained through field sampling, which is generally expensive, labour intensive, and time consuming. Further, a variety of ecological applications require data from broad spatial extents that are impossible to acquire using field-based methods [10].

Light Detection and Ranging (LiDAR) has attracted much attention from the forestry community as a rapid and efficient tool for the estimation of attributes of forest structure from the plot level to a regional scale. LiDAR systems are based on either the ranges or intensities of individual pulse returns or characterisations of the full waveform to characterise forest structure [11]. LiDAR allows ranging of objects directly by measuring the time between emitted pulses and their reflected returns. It also allows accurate measurement of forest structure from airborne, terrestrial, or spaceborne platforms through forest canopy gaps. Airborne LiDAR (or Airborne Laser Scanning, ALS) and terrestrial LiDAR (or Terrestrial Laser Scanning, TLS) have the potential to characterise the vertical structure of a forest with high-density point clouds at the stand or plot level [12].

The distribution of vertical foliage can be derived from both ALS and TLS. As an important feature, the foliage profile along the distribution of the forest canopy has been widely used to describe the distribution of the vertical structure of forests [13]. Since single spectral band LiDAR does not distinguish branches from leaves, the terms canopy height profiles (CHPs) or apparent foliage height profile are often used [14]. CHPs can be derived from large-footprint, full-waveform LiDAR systems [15,16] and small-footprint, discrete return LiDAR systems [17] as well as TLS data. Mund et al. [18] investigated the potential of full-waveform, high-density ALS data for the detection and classification of the structure of vegetation. As a key index for characterising vertical and horizontal canopy distribution, including understorey structures, the distribution of leaf area density (LAD) is enabled from ALS measurement [19]. Tang et al. [12] explored the potential of airborne waveform LiDAR for mapping vertical and horizontal distributions of leaf area index (LAI), deriving vertical profiles of LAI at 0.3 m height intervals from the Laser Vegetation Imaging Sensor (LVIS) data. TLS offers the advantage of rapidly and precisely measuring the 3D structure of the lower forest canopy and quantifying forest metrics with a high level of detail. Many studies have extracted vertical forest structure characteristics such as forest canopy gap fraction, vertical foliage profile, clumping index, and LAI with TLS data [20–22]. Danson et al. [23] used TLS to measure the distribution of canopy directional gap fractions in forest stands, finding that they were similar between hemispherical photography and TLS data, with equally high precision.

ALS data have been widely used to retrieve vertical and horizontal forest structure parameters over large areas. Nevertheless, ALS does not directly measure complete forest structure, and the canopy components of understorey layers that are occluded by the overstorey may therefore go undetected. Because transmission losses affect echo triggering probabilities and intensity observations, Korpela et al. [24] formulated a conceptual model to detect losses due to below-the-noise-level backscattering in the understorey. Although neither ALS nor TLS systems can directly provide complete information on forest structure, TLS data can measure forest structure more accurately, especially the canopy understorey [25]. TLS data can be collected only from limited field plots; however, it can be used to rebuild the 3D forest structure more precisely and provide an approach for calibrating ALS data and improving the accuracy of the estimation of forest structural variables [26–29]. Additionally, TLS data provide more spatial details of understorey forest structure than overstorey structure due to the upward-looking data collection method, making it suitable for the calibration and validation of ALS data. Over the past decade, research combining ALS and TLS data for the characterisation of forest structure has improved the detectability of foliage and biomass distribution within the forest canopy. Research utilizing ALS and TLS data from forest environments has been explored in many different

fields. For example, Wezyk et al. [30] integrated ALS and TLS data to retrieve forest inventory attributes such as tree height, diameter at breast height (DBH), basal area, crown closure, crown base height, and 2D and 3D tree crown surface with increased accuracy. Zhao et al. [31] estimated LAI and vertical foliage profile using a voxel-based method with TLS data and found that there was little difference between vertical foliage profiles retrieved from TLS, ALS, and a field survey. Greaves et al. [32] compared aboveground shrub biomass derived from TLS and ALS with an  $R^2$  value of 0.62 and found that the accuracy of ALS-derived shrub biomass predictions was the same whether they were calibrated directly against harvest biomass or against TLS-derived estimates of biomass.

Both ALS and TLS have demonstrated their potential in measuring the vertical structure of the forest canopy and the vertical distribution of the understorey layer, and their dynamics have been explored in studies. Previous research has connected CHPs from ALS and TLS layer by layer but has not taken into account overstorey shielding effects. In this study, we explored the potential advantage of linking ALS- and TLS-derived CHPs to assess changes in forest understorey volume before and after forest tending. We used detailed, plot-scale TLS understorey measurements to validate the ALS CHPs that come from both understorey and overstorey. The final objective of this study was to detect understorey changes caused by forest-tending practices in a young Khasi pine forest with a synergistic use of ALS and TLS.

## 2. Materials and Methods

### 2.1. Study Area

The study was conducted at the Wanzhangshan Forest Farm (Figure 1;  $22^{\circ}55'09''$  N,  $100^{\circ}56'51''$  E), located in Yunnan province, China. The main land cover types here are natural mixed conifer and broadleaf forest, natural broadleaf forest, young Khasi pine planted forest, and tea plantations. In the natural forest, the dominant species are Khasi pine (*Pinus kesiya*), Schima (*Schima superba* Gardner & Champ.) and Quercus glauca (*Cyclobalanopsis glauca* Oerst.). The young Khasi pine plantation is managed by the Wanzhangshan Forest Farm, with a very dense layer of shrubs and herbs in the understorey. The Khasi pine trees in the study area are no more than 6 years old, and the shrubs and herbs had never been removed before December 2013. Shrubs and herbs in the young Khasi pine stands compete for nutrients with young Khasi pine trees and are deemed an impediment to the growth of the forest plantation. In December 2013, the Wanzhangshan Forest Farm began to thin the shrub layer as well as dead and unhealthy trees.

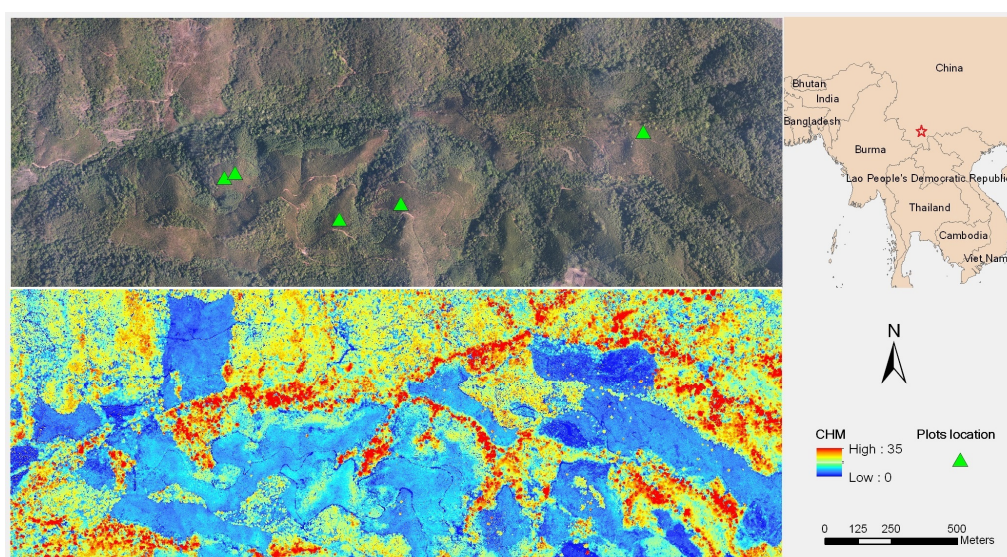


**Figure 1.** Plot locations, aerial photograph, and canopy height model (CHM) of the study area.

## 2.2. ALS Data Acquisition and Preprocessing

ALS data were acquired in December 2013 and March 2014 with a Yun-12 airplane at an altitude of approximately 1500 m. The sensor used was a RIEGL LMS-Q680i, with full-waveform data acquired [33]. The raw data were decomposed according to Gaussian decomposition models into discrete returns and georeferenced with position and orientation data. From the statistics of discrete returns in the study area, the minimum and maximum numbers of returns extracted from each waveform were 1 and 4, respectively. The discrete returns dataset thus had a maximum and minimum average point density of 6.5 pts/m<sup>2</sup> and 5.3 pts/m<sup>2</sup>, respectively. Ground and non-ground returns were separated with a ground point filter method using the software package Terrascan [34], and the elevation of LiDAR return points was normalised with respect to the ground points. At the time of the first ALS data acquisition, forest tending in the Khasi pine forest had not yet begun. However, at the time of the second ALS data acquisition, forest tending was ongoing.

## 2.3. TLS Data Acquisition and Preprocessing

The TLS data were collected using a Trimble TX8 terrestrial laser scanner (Trimble, Sunnyvale, CA, USA) in December 2013 and March 2014. The scanner uses a narrow infrared laser beam with a rapid scanning mechanism that allows rapid and non-contact data acquisition. The detection range was 120 m with a scan duration of 2–14 min. The vertical and horizontal scan angle ranges were 317° and 360°, respectively.

Due to poor visibility in the young Khasi pine forest caused by the density of the shrub layers, it is difficult to set up reference targets to register multiple scan stations, because each target should be detected by all scans. Therefore, all five plots were designed to have only one TLS scan at the plot centre. We located and marked the plot centre using differential Global Positioning System (DGPS). Within each plot, five reference targets (Figure 2) were used during scanning, allowing us to geo-register the scans using a total station and DGPS. All five targets were posted on stems that were visible to the scanner. All plots were scanned twice: before and after forest tending. The coordinates of the TLS return points were translated by DGPS using the software package Trimble RealWorks [35]. Ground and non-ground returns were separated with the same method as for ALS data, using Terrascan.



**Figure 2.** Photographs taken before (December 2013) and after (March 2014) forest tending.

## 2.4. Plot Description

Due to occlusion by shrubs and leaves before forest thinning, the recognition ability of TLS data decreased with increases in distance between the scanning equipment and the target forest stands. Therefore, we used the return points collected from forest stands within a 5-m buffer of the plot centre to extract CHPs and foliage volume in the understorey.

All young Khasi pine trees in the tending area were of the same age and therefore had very similar DBH and tree height values. When afforestation began, the forest farm planned several stand densities.

We located our plots within five different stand densities to collect TLS data. The descriptions of these plots, including manual measurements from TLS data, are shown in Table 1. For each plot, the TLS scan position was the same before and after forest tending.

**Table 1.** Description of Terrestrial Laser Scanning (TLS) plots.

ID	Number of Trees	DBH (cm)	Height (m)	Shrub and Herbage
F1	24	10	8	dense
F2	15	12	9	dense
F3	18	11	8	sparse
F4	27	8	6	dense
F5	21	10	7	dense

DBH: diameter at breast height.

## 2.5. Canopy Height Profiles Extraction

As an active remote sensing technology, the emitted laser pulse from LiDAR can penetrate the upper canopy to reach the understorey or the ground. Given this ability to accurately measure canopy structure, CHPs can be derived from LiDAR point clouds data. Extractions of most forest parameters were based on normalised point clouds to eliminate the influence of terrain on tree height. From the normalised LiDAR point clouds data, canopy height distribution can be divided into different height strata at 0.5 m intervals. Canopy cover within each stratum ( $z$ ) can then be calculated using the percentile distribution (PD) of point clouds in this stratum, as shown in Equation (1) [28]. Finally, the CHPs from the ALS data can be drawn from the PD values of all layers:

$$PD(z) = 100\% \times N(z)/N_{\text{total}} \quad (1)$$

where  $PD(z)$  is the PD of ALS return points at height  $z$  from the ground,  $N(z)$  is the number of return points in layer  $z$ , and  $N_{\text{total}}$  is the number of return points.

Conversely, terrestrial LiDAR collected more than one million return points from one position in the understorey. Due to the high point density and uneven distribution of TLS data, a voxel-based method was used to derive the CHPs of TLS data after the heights of TLS return points were normalised with ground elevation. The voxel method reduced the complexity of TLS data and permitted the characterisation of the vertical distribution of the forest canopy. Voxel size was an important parameter, and it played an important role in CHPs extraction. Large voxel size reduces the amount of canopy structure detail, whereas small voxel size may neglect important CHPs information. García et al. [36] evaluated the effects of voxel size on the estimation of degree of canopy clumping ( $\Omega$ ) by testing 5–25 cm voxels at 5 cm intervals when using TLS data. Three  $\Omega$ -estimation methods were tested for different zenith ranges. The correlation values yielded by three  $\Omega$ -estimation methods for different zenith ranges and voxel sizes were examined. Chen and Cihlar's clumping index (CCI) [37] for the 55–60 zenith range and a 5-cm voxel size yielded the strongest correlation between TLS-derived  $\Omega$  and validation  $\Omega$  extracted from hemispherical photographs. In that study, the 55–60 zenith range was the highest zenith range. Cifuentes et al. [38] inspected the effects of voxel size (ranging from 1 cm to 5 cm) and sampling design on the estimation of the forest canopy gap fraction using TLS data. The root mean square error (RMSE) of gap fraction estimates for intermediate and mature forests using point clouds at different locations (1 m, 10 m, and 14 m from the centre) decreased as voxel size increased. There was little difference in the RMSE of gap fraction estimates using point clouds at different locations from the scan centre with a 5-cm voxel size. To detect understorey volume, we used return points with larger zenith ranges. Consequently, a  $5 \times 5 \times 5$  cm voxel size was selected to extract TLS-derived CHPs with a height interval of 0.1 m from the ground to the top of the canopy. Voxels that contained more than 10 return points were designated filled voxels.

## 2.6. Understorey Volume Estimates and Changes Detected after Forest Tending

The main objective of forest tending was to remove shrubs, grasses, and unhealthy or dead trees. Because the height of the TLS scan station was approximately 1.5 m, it more precisely detected the understorey than the overstorey. To estimate understorey volume and detect any change in volume after forest tending in the young Khasi pine forest, CHPs were separated into ground, overstorey, and understorey layers according to the CHPs before and after forest tending.

Because most materials removed after forest tending were in the understorey, the variation of CHPs referred to the change of understorey distribution. A threshold height was chosen to separate understorey and overstorey according to the variation in all CHPs in this study. The threshold height was the height below which substantial material was removed and above which material was rarely removed. After forest tending, all removed material was piled on the ground to a height of approximately 0.5 m. For this reason, we defined 0.5 m as the threshold height for separating the ground and understorey layers. Therefore, the ground layer included grasses and short shrubs as well as bare ground before forest tending and shrub debris after forest tending.

The understorey volume, calculated using the number of filled TLS voxels, was considered the reference value. The change in understorey volume was calculated from the understorey volume before and after forest tending.

ALS-derived PD of the overstorey and understorey layers were calculated to compare to the TLS-derived understorey volume. We used two methods to compare the understorey volume according to TLS and the PD according to ALS. First, we directly compared the PD values according to ALS from the understorey (Equation (1)) with the understorey volume according to TLS. However, the detectability of understorey PD values from ALS was heavily impacted by the shading effects of the overstorey. In addition to the greater numbers of branches and leaves in the overstorey, higher PD values for the overstorey also indicated stronger shading effects. PD values for the z layer were related to the amount of branches and leaves in this layer and in the overstorey canopy cover (above the z layer). Therefore, we used a weighted PD value to compare that of the understorey volume in TLS (Equation (2)):

$$PD_{Weighted}(z) = PD(z) \times PD(h > z) \quad (2)$$

where  $PD(h > z)$  is the PD of ALS return points above height stratum  $z$ , or the degree of canopy closure above height  $z$ .

Within canopy height distribution in the understorey, the PD from ALS and weighted PD from ALS were expressed as follows:

$$PD(Understorey) = 100\% \times N(Understorey) / N_{total} \quad (3)$$

$$PD_{Weighted}(Understorey) = PD(Understorey) \times PD(Overstory) \quad (4)$$

$$TLS_{volume}(Understorey) = \sum_{z=0.5}^{z=H} N_{Filled-Voxel} \times 0.05 \times 0.05 \times 0.05 \quad (5)$$

where the PD values are calculated using ALS return points.  $H$  is the threshold height that separates the understorey and overstorey layers in all plots.  $N_{Filled-Voxel}$  is the number of filled TLS voxels.

Because all five field plots were scanned by ALS and TLS before and after forest tending events, 10 ALS–TLS data pairs were extracted from the field plots. The model was developed from the relationship between the TLS-estimated volume and ALS PD values or weighted understorey PD values for the 10 ALS–TLS data pairs, and leave-one-out cross-validation was performed to evaluate model performance. For each cross-validation split, one sample was tested, using the predictor model derived from the nine remaining samples. The cross-validated coefficient of determination ( $R^2$ ) and RMSE were calculated. Volume changes in the understorey after forest tending in the young Khasi pine forest area were calculated based on the model built from all 10 samples.

### 3. Results

#### 3.1. Comparison of Canopy Height Profiles

According to the CHPs in Figure 3, the canopy in these plots was separated into three layers: ground (under 0.5 m), understorey (0.5–3.5 m), and overstorey (above 3.5 m). As shown by the CHPs from TLS in Figure 3, a substantial change in the number of filled voxels occurred between 0.5 m and 3.5 m along the canopy height distribution. This change can be attributed to the effects of forest tending activities in young Khasi pine forest. The forest canopy understorey became more open and occlusion by shrubs was reduced following forest tending. Consequently, the number of filled voxels for the CHPs from TLS decreased in the understorey and increased in the overstorey after forest tending.

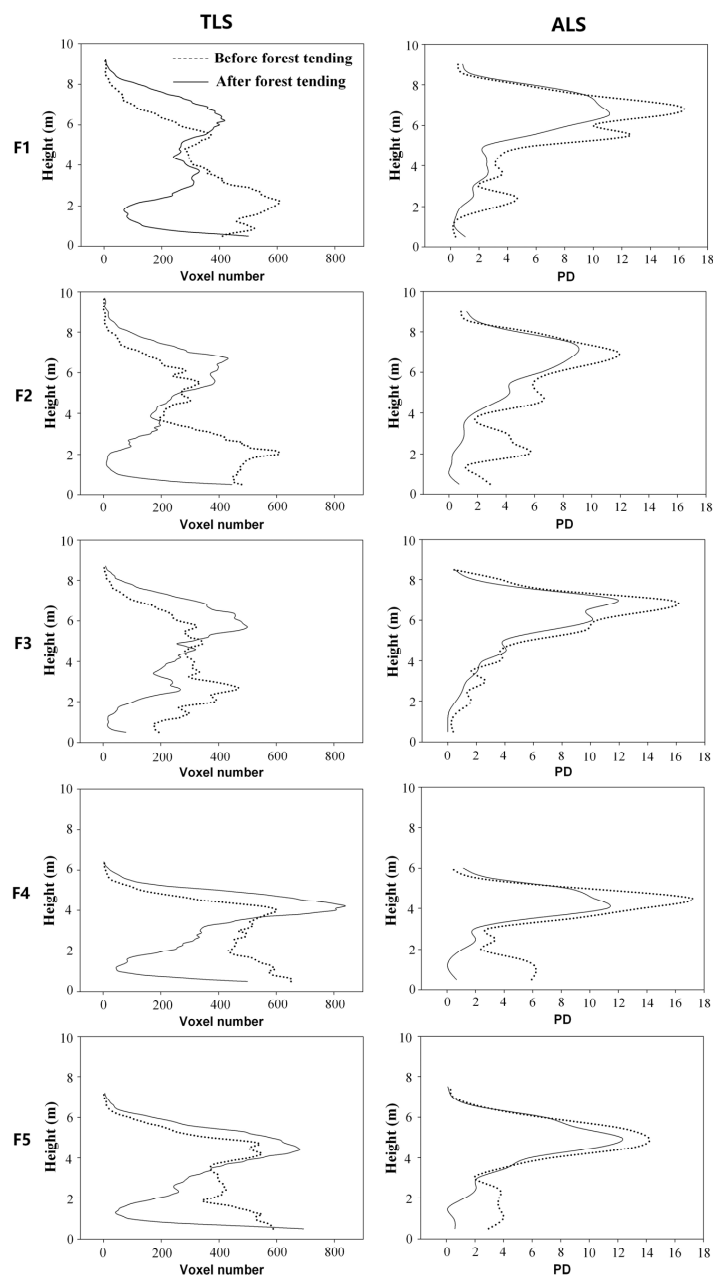


**Figure 3.** Canopy height profiles (CHPs) in plots from Terrestrial Laser Scanning (TLS) and Airborne Laser Scanning (ALS) data before and after forest tending. The CHPs from TLS were drawn from the number of filled voxels at every layer (0.1 m interval), and the CHPs from ALS were drawn using the percentile distribution of return points at every layer (0.5 m interval).

In contrast to the CHPs from TLS, the CHPs from ALS had higher values in the understorey and overstorey before forest tending than after forest tending. This is because shrubs and grasses in the understorey and unhealthy and dead trees in the overstorey were cleared during forest tending. Forest tending in the understorey made the identification of unhealthy and dead standing trees easier than it had been previously. There were very few leaves on unhealthy and dead standing trees; therefore, only a small proportion of the overstorey volume had been removed. However, the PD value for the ALS return points showed a much stronger foliage volume change in the overstorey than in the understorey. Because canopy cover was calculated using the percentage of ALS return points in the overstorey, the laser reached the ground or understorey more frequently after forest tending. Therefore, the percentage of overstorey return points before forest tending was much greater than that after forest tending. The same area of change under the understorey CHPs from ALS indicated greater removed volume than from the overstorey. In plot F3, with a less dense shrub and grass layer, the change in CHPs from ALS after forest tending was not as significant as in plots with a dense shrub and grass layer.

### 3.2. Mapping Understorey Changes Following Forest Tending

As shown in Figure 4, linear regressions were performed between PD according to ALS or weighted PD value and TLS understorey filled-voxel volume (from 0.5 m to 3.5 m along the canopy height). The plots that were scanned before and after forest tending are indicated in white and black, respectively. The correlation of the weighted PD value from ALS and the TLS-derived volume ( $R^2 = 0.9$ ,  $p < 0.01$ ) in the understorey was stronger than that of the unweighted PD value from ALS ( $R^2 = 0.71$ ,  $p < 0.01$ ). The PD value for the understorey in plots with denser overstorey canopy cover tended to be underestimated more than plots with open overstorey canopy cover (Figure 4a). These results demonstrated that the overstorey PD value for ALS return points influenced the detectability of the understorey PD. The weighted PD value from ALS is therefore useful for estimating understorey volume.

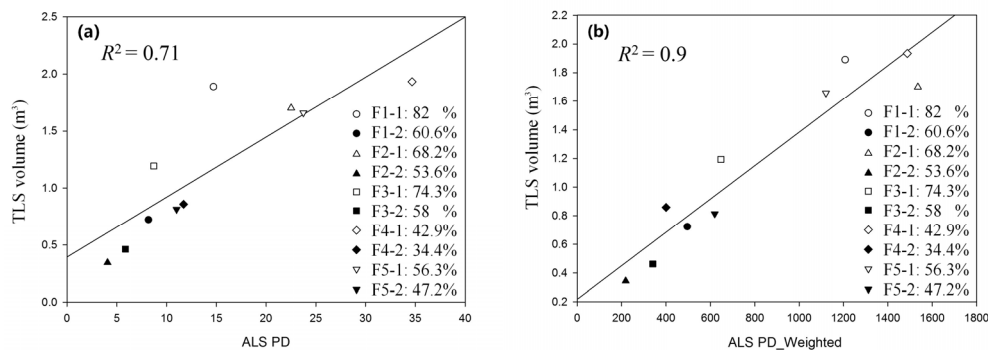


**Figure 4.** Comparison of PD (a), weighted PD (b) from Airborne Laser Scanning (ALS) and Terrestrial Laser Scanning (TLS)-derived volume in the understorey. White and black scatter points are the five plots before and after forest tending, respectively. In the legend, all plots are marked by different percentile distribution (PD) values for the ALS return points in the overstorey. Before forest tending, plot F1 had the greatest overstorey canopy cover (82%), as calculated using the percentage of return points in ALS in the overstorey.

Because ALS-weighted PD values were more strongly correlated with TLS-filled voxel volume in the understorey, the predicted model of understorey volume was developed using ALS-weighted PD values and leave-one-out cross-validation was performed. The adjusted  $R^2$  and RMSE of the 10 models ranged from  $0.87 \text{ m}^3$  to  $0.94 \text{ m}^3$  and  $0.16 \text{ m}^3$  to  $0.21 \text{ m}^3$ . Figure 5 shows the relationship between TLS-measured and ALS-predicted understorey volumes using leave-one-out cross-validation.

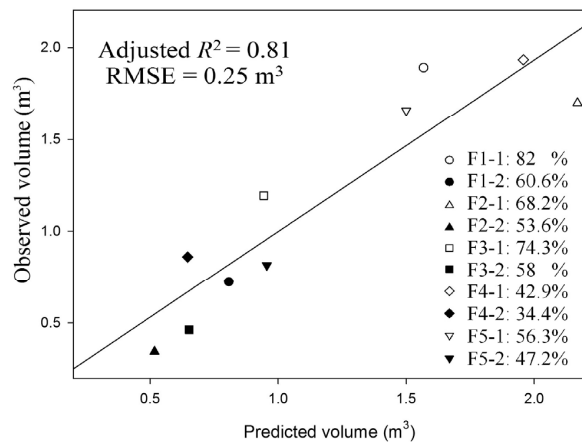


**Figure 5.** The Terrestrial Laser Scanning-measured (observed) versus predicted understorey volume by Airborne Laser Scanning-weighted percentile distribution values (calibrated using leave-one-out cross-validation).

Finally, to build understorey volume maps, a linear model was established using ALS-weighted PD values and TLS-estimated understorey volume from all 10 samples from the Khasi pine forest farm. The model was applied with 5 m resolution using bi-temporal ALS data (Figure 6). The understorey volume removed was calculated as the difference in volume before and after forest tending. The distribution of and variation in understorey volume were estimated by multi-temporal LiDAR remote sensing.

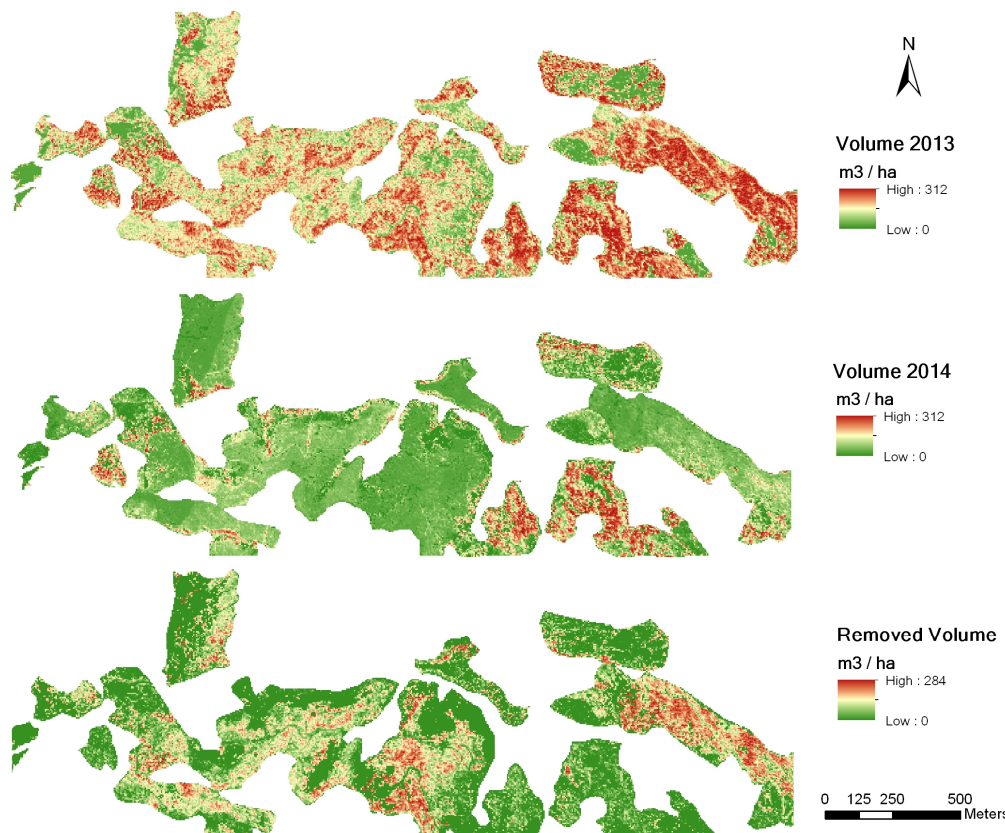


**Figure 6.** The distribution of understorey volume before and after forest tending, and the variation in understorey volume caused by forest tending.

#### 4. Discussion

Canopy structure is a fundamental property of forest ecosystems. Canopy structure can influence microclimate, runoff, forest disturbance, and biodiversity. A traditional approach to quantifying the canopy vertical structure is to map and measure trees by species, vertical stratification, and canopy class through manual fieldwork [39]. To determine the distribution of forest canopy cover among strata of forest height, field surveys are quite appropriate to assess canopy vertical structure measurements; however, they are also labour-intensive, scale-dependent, and time-consuming. Remote sensing data and techniques, especially LiDAR, have been used to characterise forest canopy vertical structure from the plot level to regional scales [40]. However, as part of forest canopy structure, the understorey has rarely been well explored.

We explored the relationship between ALS- and TLS-derived CHPs in the understorey. ALS- and TLS-derived CHPs of all plots before and after forest tending were extracted. Figure 3 shows that TLS observations have the advantage of characterising more details in understorey vegetation than in the overstorey. By contrast, ALS-derived data collectively can describe canopy height distribution in the overstorey better than TLS observations, whereas the vegetation components in the understorey are illustrated with less detail. A study by Hancock et al. [41] yielded a result that our study supports, that TLS-derived vegetation density at the canopy top was underestimated compared to that derived by ALS. Chasmer et al. [29] examined the voxel column PD at the plot level for ALS and TLS. That study demonstrated that for ALS, a high percentage of laser pulses was intercepted by the top of the canopy with fewer returns from within the canopy and understorey; similarly, for TLS, a high percentage of laser pulses were intercepted by the understorey, stems, and lower canopy, with a lower percentage of pulses reaching the upper canopy. This study and previous research has shown that both ALS and TLS data can represent the vertical distribution of the forest canopy, while also showing the inability of ALS data to characterise understorey vegetation structure in detail. It is meaningful to use TLS data to validate ALS understorey vegetation structure estimates, because TLS shows much more understorey detail than ALS.

For most plots, the understorey volume was underestimated before forest tending compared to post-forest tending, due to the removal of dead or stressed trees. Because the crowns of removed trees were piled on the ground, more laser points penetrated the overstorey to reach the understorey. Although CHPs from both TLS and ALS were incapable of representing the complete vertical structure of the canopy due to occlusion, the canopy component within one layer was extracted by ALS and TLS data with a high coefficient of determination ( $R^2 = 0.71$ ).

In previous research, the relationship between ALS- and TLS-derived CHPs has been examined without considering the overstorey [28,30]. In this study, we combined the PD values for return points in the overstorey and understorey. The relationship between ALS- and TLS-derived canopy component distributions in the understorey became stronger, with the  $R^2$  increasing from 0.71 to 0.90. Linear regression was performed and an assessment using leave-one-out cross-validation showed an excellent result, with an adjusted  $R^2$  and RMSE of  $0.81 \text{ m}^3$  and  $0.25 \text{ m}^3$ , respectively. This result is important, because it illustrates the capacity of ALS and TLS data to be used for volume estimation in the understorey.

We used the estimated canopy volume to detect variation in the volume of foliage in the understorey. We did not design an experiment to evaluate the relationship between TLS-derived volume and field harvest biomass. In our estimation of the canopy volume of the understorey using ALS data, the volume of the canopy component estimated with filled TLS voxels was used as verification data. Traditionally, ALS data are calibrated against field data to estimate aboveground biomass. To calibrate the biomass of shrubs in the understorey, destructive harvesting is a simple method; however, destructive harvesting is limited by multitemporal and multiscale sampling. TLS provides a potential alternative approach for the calibration of ALS data without destructive harvesting [23,31]. Greaves et al. [42] showed that TLS-derived canopy volume provides a robust proxy to shrub biomass in Arctic tundra. In one of their other studies, aboveground shrub biomass was derived by both ALS and TLS data [32]. In that study, TLS produced more accurate predictions

of shrub biomass ( $R^2 = 0.78$ , validated by harvested sampling) than did ALS; however, the accuracy of ALS-derived shrub biomass predictions ( $R^2 = 0.62$ ) was identical when calibrated directly against harvested biomass and TLS-derived estimates of biomass. The authors suggested that once the initial TLS–harvest relationship was known, TLS could provide validation data for ALS shrub biomass estimation without additional destructive harvesting. Few harvesting samples are needed in specific areas to provide validation data for vegetation structure estimation of the understorey by TLS. Therefore, TLS data have the potential to provide validation data for ALS understorey vegetation structure estimates at regional scales without harvesting samples.

It was difficult to set up multiple TLS scans in the young Khasi pine forest due to the dense understorey shrub layer. Despite this obstacle, there was strong agreement between CHPs from ALS and TLS derived from a single scan in the understorey. Multiple-scan TLS data can describe understorey structure in greater detail. TLS would thus constitute a better validation tool in forested areas where setting up multiple TLS scans is easier. For example, Li et al. [43] used multi-scan TLS-derived shrub biomass to calibrate a biomass prediction model of ALS-derived percent vegetation cover with a better validation result ( $R^2 = 0.87$ ) than obtained in this study ( $R^2 = 0.81$ ).

Our method applied estimates of understorey volume under different ALS point densities using a full-waveform system. Both ALS data showed strong agreement with TLS data. Point density was generally related to the ability to estimate forest structure, with high-density ALS data having greater potential to extract forest structure. However, this argument is not appropriate for ALS data from different sensors, such as discrete-return and full-waveform LiDAR. Discrete-return LiDAR uses proprietary algorithms to produce point clouds and can be biased over vegetation [44]. Full-waveform LiDAR measures the reflected laser intensity as a function of range, which can depict the full dimension of the target objects [45]. This study estimated understorey volume and its changes due to forest tending. Unlike discrete-return LiDAR, full-waveform LiDAR offers the potential to measure understorey structure at the resolution of ALS footprint density. The CHPs-based method may not be appropriate for understorey volume estimation using discrete-return LiDAR data (especially first return only) with low-density points in forests with dense canopy cover.

The methods used in our study have great potential for monitoring forest understorey dynamics before and after forest tending activities. The removal of understorey volume due to forest tending can be quantified based on the model developed from TLS and ALS data. In contrast to fine-scale, detailed examination of understorey structure using the TLS technique, ALS remote sensing has the advantage of broad-scale assessment of CHPs over larger areas. Furthermore, ALS data provide greater credibility in quantifying overstorey PDs of return points. Our study found that differences in overstorey canopy cover influenced the understorey volume estimate from ALS data. This finding could help improve the accuracy of ALS-based understorey volume detection by integrating the overstorey canopy cover into the modelling process. It could also improve the development of data collection, specification, and calibration of ALS-derived understorey height distributions through ALS. Shrub and grass cover in the forest understorey plays an important role in forest ecology by providing significant wildlife habitat, modifying soil nutrient cycles, and contributing to forest carbon sequestration. An accurate quantification of disturbance in understorey shrub and grass layers has significant implications for forest diversity and the modelling of forest growth, stand development, and forest succession [46].

## 5. Conclusions

This study assessed the agreement between understorey CHPs retrieved from ALS return points with those retrieved from filled TLS voxels in a young Khasi pine forest. The comparison of CHPs from the coarser spatial resolution, downward-looking ALS system with the finer, upward-looking TLS system showed good correlation in understorey volume. We did not estimate the volume of grasses and shrubs below a threshold 0.5 m above the ground, because their volume could be confused with removed plant material piled on the ground following forest tending. With the help of TLS data, CHPs extracted using ALS data could be quantified and converted to corresponding forest structure

attributes for a large area. Although there is no harvested sampling to verify understorey volume estimates, integrating ALS and TLS data showed great potential for detecting changes in attributes of the understorey canopy of forests.

**Acknowledgments:** This work was supported by National Basic Research Program of China (2013CB733404 and 2013CB733406). The authors are grateful to Xuan Guo, Giona Matasci, Tristan Goodbody, and Yuhao Lu for their editorial assistance and constructive comments which helped improve the quality of this paper.

**Author Contributions:** L.Z. and P.Y. conceived and designed the ideal of paper; L.L., S.L. and L.S. performed the experiments; L.L. analysed the data and wrote the paper.

**Conflicts of Interest:** The authors declare no conflicts of interest.

## References

1. D'Amato, A.W.; Orwig, D.A.; Foster, D.R. Understory vegetation in old-growth and second-growth *Tsuga canadensis* forests in western Massachusetts. *For. Ecol. Manag.* **2009**, *257*, 1043–1052. [[CrossRef](#)]
2. Halpern, C.; Spies, T. Plant species diversity in natural and managed forests of the Pacific Northwest. *Ecol. Appl.* **1995**, *5*, 913–934. [[CrossRef](#)]
3. Gonzalez, M.; Augusto, L.; Gallet-Budynek, A.; Xue, J.; Yauschew-Raguenes, N.; Guyon, D.; Trichet, P.; Delerue, F.; Niollet, S.; Andreasson, F.; et al. Contribution of understory species to total ecosystem aboveground and belowground biomass in temperate *Pinus pinaster* Ait. forests. *For. Ecol. Manag.* **2013**, *289*, 38–47. [[CrossRef](#)]
4. Cook, J.E. Structural effects on understory attributes in second-growth forests of northern Wisconsin, USA. *For. Ecol. Manag.* **2015**, *347*, 188–199. [[CrossRef](#)]
5. McCarthy, N.; Bentzen, N.S.; Willoughby, I.; Balandier, P. The state of forest vegetation management in Europe in the 21st century. *Eur. J. For. Res.* **2011**, *130*, 7–16. [[CrossRef](#)]
6. Barbier, S.; Gosselin, F.; Balandier, P. Influence of tree species on understory vegetation diversity and mechanisms involved—A critical review for temperate and boreal forests. *For. Ecol. Manag.* **2008**, *254*, 1–15. [[CrossRef](#)]
7. Yarie, J. The Role of Understory Vegetation in the Nutrient Cycle of Forested Ecosystems in the Mountain Hemlock Biogeoclimatic Zone. *Ecology* **1980**, *61*, 1498–1514. [[CrossRef](#)]
8. Montgomery, R.A.; Chazdon, R.L. Forest structure, canopy architecture, and light transmittance in tropical wet forests. *Ecology* **2001**, *82*, 2707–2718. [[CrossRef](#)]
9. Pelt, R.V.; Franklin, J.F. Influence of canopy structure on the understory environment in tall, old-growth, conifer forests. *Can. J. For. Res.* **2000**, *30*, 1231–1245. [[CrossRef](#)]
10. Kerr, J.T.; Ostrovsky, M. From space to species: Ecological applications for remote sensing. *Trends Ecol. Evolut.* **2003**, *18*, 299–305. [[CrossRef](#)]
11. Wulder, M.A.; Bater, C.W.; Coops, N.C.; Hilker, T.; White, J.C. The role of LiDAR in sustainable forest management. *For. Chron.* **2008**, *84*, 807–826. [[CrossRef](#)]
12. Tang, H.; Dubayah, R.; Swatantran, A.; Hofton, M.; Sheldon, S.; Clark, D.B.; Blair, B. Retrieval of vertical LAI profiles over tropical rain forests using waveform lidar at La Selva, Costa Rica. *Remote Sens. Environ.* **2012**, *124*, 242–250. [[CrossRef](#)]
13. MacArthur, R.H.; Horn, H.S. Foliage Profile by Vertical Measurements. *Ecology* **1969**, *50*, 802–804. [[CrossRef](#)]
14. Coops, N.C.; Hilker, T.; Wulder, M.A.; St-Onge, B.; Newnham, G.; Siggins, A.; Trofymow, J.A. Estimating canopy structure of Douglas-fir forest stands from discrete-return LiDAR. *Trees* **2007**, *21*, 295–310. [[CrossRef](#)]
15. Lefsky, M.A.; Cohen, W.B.; Acker, S.A.; Parker, G.G.; Spies, T.A.; Harding, D. Lidar remote sensing of the canopy structure and biophysical properties of Douglas-fir western hemlock forests. *Remote Sens. Environ.* **1999**, *70*, 339–361. [[CrossRef](#)]
16. Harding, D.J.; Lefsky, M.A.; Parker, G.G.; Blair, J.B. Laser altimeter canopy height profiles methods and validation for closed-canopy, broadleaf forests. *Remote Sens. Environ.* **2001**, *76*, 283–297. [[CrossRef](#)]
17. Fieber, K.D.; Davenport, I.J.; Tanase, M.A.; Ferryman, J.M.; Gurney, R.J.; Becerra, V.M.; Walker, J.P.; Hacker, J.M. Validation of Canopy Height Profile methodology for small-footprint full-waveform airborne LiDAR data in a discontinuous canopy environment. *ISPRS J. Photogramm. Remote Sens.* **2015**, *104*, 144–157. [[CrossRef](#)]

18. Mund, J.; Wilke, R.; Körner, M.; Schultz, A. Detecting Multi-layered Forest Stands Using High Density Airborne LiDAR Data. *J. Geogr. Inf. Sci.* **2015**. [[CrossRef](#)]
19. Lin, Y.; West, G. Retrieval of effective leaf area index (LAIe) and leaf area density (LAD) profile at individual tree level using high density multi-return airborne LiDAR. *Int. J. Appl. Earth Obs. Geoinf.* **2016**, *50*, 150–158. [[CrossRef](#)]
20. Ramirez, F.A.; Armitage, R.P.; Danson, F.M. Testing the application of terrestrial laser scanning to measure forest canopy gap fraction. *Remote Sens.* **2013**, *5*, 3037–3056. [[CrossRef](#)]
21. Strahler, A.H.; Jupp, D.L.B.; Woodcock, C.E.; Schaaf, C.B.; Yao, T.; Zhao, F.; Yang, X.; Lovell, J.; Culvenor, D.; Newnham, G.; et al. Retrieval of forest structural parameters using a ground-based lidar instrument (Echidna®). *Can. J. Remote Sens.* **2008**, *34*, 426–440. [[CrossRef](#)]
22. Zheng, G.; Moskal, L.M. Computational-geometry-based retrieval of effective leaf area index using terrestrial laser scanning. *IEEE Trans. Geosci. Remote Sens.* **2012**, *50*, 3958–3969. [[CrossRef](#)]
23. Danson, F.M.; Hetherington, D.; Morsdorf, F.; Koetz, B.; Allgower, B. Forest canopy gap fraction from terrestrial laser scanning. *IEEE Geosci. Remote Sens. Lett.* **2007**, *4*, 157–160. [[CrossRef](#)]
24. Korpela, I.; Hovi, A.; Morsdorf, F. Understory trees in airborne LiDAR data—Selective mapping due to transmission losses and echo-triggering mechanisms. *Remote Sens. Environ.* **2012**, *119*, 92–104. [[CrossRef](#)]
25. Seidel, D.; Albert, K.; Fehrmann, L.; Ammer, C. The potential of terrestrial laser scanning for the estimation of understory biomass in coppice-with-standard systems. *Biomass Bioenergy* **2012**, *47*, 20–25. [[CrossRef](#)]
26. Chasmer, L.; Hopkinson, C.; Treitz, P. Investigating laser pulse penetration through a conifer canopy by integrating airborne and terrestrial lidar. *Can. J. Remote Sens.* **2006**, *32*, 116–125. [[CrossRef](#)]
27. Jung, S.-E.; Kwak, D.-A.; Park, T.; Lee, W.-K.; Yoo, S. Estimating Crown Variables of Individual Trees Using Airborne and Terrestrial Laser Scanners. *Remote Sens.* **2011**, *3*, 2346–2363. [[CrossRef](#)]
28. Hopkinson, C.; Lovell, J.; Chasmer, L.; Jupp, D.; Kljun, N.; van Gorsel, E. Integrating terrestrial and airborne lidar to calibrate a 3D canopy model of effective leaf area index. *Remote Sens. Environ.* **2013**, *136*, 301–314. [[CrossRef](#)]
29. Chasmer, L.; Hopkinson, C.; Treitz, P. Assessing the three-dimensional frequency distribution of airborne and ground-based lidar data for red pine and mixed deciduous forest plots. In Proceedings of the Laser Scanners for Forest and Landscape Assessment—Instruments, Processing Methods and Applications, Freiburg, Germany, 3–6 October 2004.
30. Wezyk, P. The integration of the Terrestrial and Airborne Laser Scanning technologies in the semi-automated process of retrieving selected trees and forest stand parameters. *Ambiencia* **2012**, *8*, 533–548.
31. Zhao, F.; Yang, X.; Strahler, A.H.; Schaaf, C.L.; Yao, T.; Wang, Z.; Román, M.O.; Woodcock, C.E.; Ni-Meister, W.; Jupp, D.L.B.; et al. A comparison of foliage profiles in the Sierra National Forest obtained with a full-waveform under-canopy EVI lidar system with the foliage profiles obtained with an airborne full-waveform LVIS lidar system. *Remote Sens. Environ.* **2013**, *136*, 330–341. [[CrossRef](#)]
32. Greaves, H.E.; Vierling, L.A.; Eitel, J.U.H.; Boelman, N.T.; Magney, T.S.; Prager, C.M.; Griffin, K.L. Applying terrestrial lidar for evaluation and calibration of airborne lidar-derived shrub biomass estimates in Arctic tundra. *Remote Sens. Lett.* **2017**, *8*, 175–184. [[CrossRef](#)]
33. Pang, Y.; Li, Z.; Ju, H.; Lu, H.; Jia, W.; Si, L.; Guo, Y.; Liu, Q.; Li, S.; Liu, L.; et al. LiCHy: The CAF’s LiDAR, CCD and Hyperspectral Integrated Airborne Observation System. *Remote Sens.* **2016**, *8*, 398. [[CrossRef](#)]
34. Terra solid POINT CLOUD INTELLIGENCE. Available online: [https://www.terrasolid.com/products/terrascan\\_versionhistory.php](https://www.terrasolid.com/products/terrascan_versionhistory.php) (accessed on 17 January 2017).
35. Trimble RealWorks. Available online: <https://www.trimble.com/3d-laser-scanning/realworks.aspx> (accessed on 17 January 2017).
36. García, M.; Gajardo, J.; Riaño, D.; Zhao, K.; Martín, P.; Ustin, S. Canopy clumping appraisal using terrestrial and airborne laser scanning. *Remote Sens. Environ.* **2015**, *161*, 78–88. [[CrossRef](#)]
37. Chen, J.M.; Cihlar, J. Plant canopy gap-size analysis theory for improving optical measurements of leaf-area index. *Appl. Opt.* **1995**, *34*, 6211–6222. [[CrossRef](#)] [[PubMed](#)]
38. Cifuentes, R.; Van der Zande, D.; Farifteh, J.; Salas, C.; Coppin, P. Effects of voxel size and sampling setup on the estimation of forest canopy gap fraction from terrestrial laser scanning data. *Agric. For. Meteorol.* **2014**, *194*, 230–240. [[CrossRef](#)]
39. Schulze, C.H.; Linsenmair, K.E.; Fiedler, K. Understorey versus canopy: Patterns of vertical stratification and diversity among Lepidoptera in a Bornean rain forest. *Trop. For. Canopies Ecol. Manag.* **2001**, *153*, 133–152.

40. Guo, X.; Coops, N.C.; Tompalski, P.; Nielsen, S.E.; Bater, C.W.; Stadt, J.J. Regional mapping of vegetation structure for biodiversity monitoring using airborne lidar data. *Ecol. Inform.* **2017**, *38*, 50–61. [[CrossRef](#)]
41. Hancock, S.; Anderson, K.; Disney, M.; Gaston, K.J. Measurement of fine-spatial-resolution 3D vegetation structure with airborne waveform lidar: Calibration and validation with voxelised terrestrial lidar. *Remote Sens. Environ.* **2017**, *188*, 37–50. [[CrossRef](#)]
42. Greaves, H.E.; Vierling, L.A.; Eitel, J.U.H.; Boelman, N.T.; Magney, T.S.; Prager, C.M.; Griffin, K.L. Estimating aboveground biomass and leaf area of low-stature Arctic shrubs with terrestrial LiDAR. *Remote Sens. Environ.* **2015**, *164*, 26–35. [[CrossRef](#)]
43. Li, A.; Glenn, N.F.; Olsoy, P.J.; Mitchell, J.J.; Shrestha, R. Aboveground biomass estimates of sagebrush using terrestrial and airborne LiDAR data in a dryland ecosystem. *Agric. For. Meteorol.* **2015**, *213*, 138–147. [[CrossRef](#)]
44. Disney, M.I.; Kalogirou, V.; Lewis, P.; Prieto-Blanco, A.; Hancock, S.; Pfeifer, M. Simulating the impact of discrete-return lidar system and survey characteristics over young conifer and broadleaf forests. *Remote Sens. Environ.* **2010**, *114*, 1546–1560. [[CrossRef](#)]
45. Anderson, K.; Steven, H.; Mathias, D.; Kevin, J.G. Is waveform worth it? A comparison of LiDAR approaches for vegetation and landscape characterization. *Remote Sens. Ecol. Conserv.* **2015**, *2*, 5–15. [[CrossRef](#)]
46. Royo, A.A.; Carson, W.P. On the formation of dense understory layers in forests worldwide: Consequences and implications for forest dynamics, biodiversity, and succession. *Can. J. For. Res.* **2006**, *36*, 1345–1362. [[CrossRef](#)]



© 2017 by the authors. Licensee MDPI, Basel, Switzerland. This article is an open access article distributed under the terms and conditions of the Creative Commons Attribution (CC BY) license (<http://creativecommons.org/licenses/by/4.0/>).